Optimization of laser-focused deposition lines: Rydberg atoms

Cite as: J. Chem. Phys. **125**, 024703 (2006); https://doi.org/10.1063/1.2212392
Submitted: 04 April 2005 • Accepted: 16 May 2006 • Published Online: 13 July 2006

Nam A. Nguyen, Moshe Shapiro and Paul Brumer

Optimization of laser-focused deposition lines: Rydberg atoms

Nam A. Nguyen[a)]
Chemical Physics Theory Group, Department of Chemistry, University of Toronto, Toronto, Ontario M5S 3H6, Canada and Center for Quantum Information and Quantum Control, University of Toronto, Toronto, Ontario M5S 3H6, Canada

Moshe Shapiro
Chemical Physics Department, Weizmann Institute of Science, Rehovot 76100, Israel; Department of Chemistry, University of British Columbia, Vancouver V6T 1Z1, Canada; and Department of Physics and Astronomy, University of British Columbia, Vancouver V6T 1Z1, Canada

Paul Brumer[b)]
Chemical Physics Theory Group, Department of Chemistry, University of Toronto, Toronto, Ontario M5S 3H6, Canada and Center for Quantum Information and Quantum Control, University of Toronto, Toronto, Ontario M5S 3H6, Canada

(Received 4 April 2005; accepted 16 May 2006; published online 13 July 2006)

Optimally narrow nanoscale lines are computationally obtained for Rb Rydberg atoms deposited on surfaces. The use of optimized polychromatic fields is shown to allow lines as narrow as 1 nm in the absence of transverse velocities and shown to counter the deleterious effects of transverse velocities in laser cooled beams. Specifically, lines as narrow as 6.5 nm wide are obtained in the presence of transverse velocities associated with a temperature of 1 mK. Using this approach it is possible to deposit a single narrow line, even when the atomic beam is bigger than the period of the focusing lens, using as few as two, relatively weak, laser fields. © *2006 American Institute of Physics*.
[DOI: 10.1063/1.2212392]

I. INTRODUCTION

Strong demand for faster electronic devices has been the main driving force behind rapid developments in microelectronics. Although the density of circuits has been increasing steadily, the principle of the fabrication procedure remains unchanged: optical lithography. Here one patterns a surface by irradiating a mask, leading to photochemical processes on the surface, and then removes the photochemically nonreacted region. The current rate of miniaturization cannot, however, be sustained indefinitely because both the size of the atoms deposited on a surface and the diffraction of the light source impose physical limitations on the resolution of optical lithography.[1] A number of approaches are being explored to circumvent this limitation and to allow for the fabrication of electronic devices at the nanoscale. One of these, nanolithography, has its origin in the field of atom optics. Specifically, in atom nanolithography,[2–10] as in atom trapping,[11] one relies on the dipole force (the force due to the interaction of the atom's induced dipole moment with an inhomogeneous electric field) to direct the atomic motion. Recently, efforts have been made to extend nanolithography to include molecules.[12–14]

Nanolithography differs from traditional optical lithography in using an atomic beam as the material source and laser light as a focusing lens. A beam of atoms, aimed at a substrate, passes through a laser beam that exerts a force dependent on the characteristics of the light. The process is direct write, thus causing less physical damage to the surface. In addition, nanolithography allows for a parallel fabrication of deposition patterns if one designs the laser light to form an array of lenses.

Despite recent success, it is difficult to produce arbitrary patterns[15,16] in nanolithography. Recently, we introduced a degree of flexibility in nanolithographic patterns by using coherent control[18] to introduce nonperiodicity into the nanoscale pattern formation. This approach was successfully applied (computationally) to the N_2 molecule[17] and to neutral Rydberg atoms.[19] In doing so one sees clearly that the basic mechanism in all control scenarios in nanolithography is the manipulation of the light-induced potential (LIP), which is the product of the applied electric field with the atom's induced dipole moment. It is this LIP, whose gradient is the dipole force, that governs the motion of the atoms' centers of mass. In coherent control, manipulation of the LIP (Refs. 17 and 19) is achieved by altering the dynamic polarizability of the atom using interference between different optical excitation pathways. However, the LIP can also be manipulated, as shown further in this paper, by varying the external electric fields' parameters such as frequencies, phases, and intensities of polychromatic fields to tailor them to give a desired deposition pattern on a surface.

The primary goal of this paper is to introduce a method of producing high-contrast deposition patterns that consist of a sharp peak and a reduced background (pedestal) using relatively weak fields, even when the atomic beam is larger than the period of the focusing lens. In some sense these single lines can be regarded as the fundamental building block of arbitrary surface patterns.

[a)]Present address: Département de Chimie, Université de Sherbrooke, Sherbrooke, Québec J1K 2R1, Canada.
[b)]Electronic mail: pbrumer@tikva.chem.utoronto.ca

In order to achieve this goal, Rydberg atoms are used as the material source. Such atoms possess large polarizabilities, allowing for effective light-induced potential using relatively low intensity fields. Furthermore, they have unusually long lifetimes, allowing a longer interaction time between the atomic beam and the laser fields.

There is a growing number of applications that take advantage of novel properties of Rydberg states (for a review see Ref. 20). Of particular interest is that the deflection of rubidium Rydberg atoms was demonstrated experimentally by using crossed electric and magnetic fields.[21,22] Furthermore, it has been shown recently, both theoretically and experimentally, that one can control the translational motion of Rydberg molecules.[23–25] The creation of atom optical elements based on the polarizability of highly excited Rydberg states in an electric field has also been demonstrated.[26] These successful studies open the opportunity of employing Rydberg atoms and molecules in nanolithography.

Note also that dealing with Rydberg atoms is computationally straightforward since they can be treated as quasihydrogenic atoms.[27,28] Here we focus on Rydberg states of rubidium, although other alkalis can be treated as readily.

In order to deal with multiple field scenarios we utilize optimal control theory, which has been used widely in electrical and mechanical engineering for decades.[29] It has been adapted to the field of laser-matter interaction[30] to control the branching ratios of different reaction channels,[31] the photodissociation and ionization yields,[32] the shape of a quantum wave function,[33] and the alignment of molecules,[34] demonstrating the viability of optimal control in quantum dynamics. This approach then identifies the field parameters that optimize the single narrow line target.

There exist a few sources of linewidth degradation, of which the transverse velocity distribution due to an imperfect collimation by transverse laser cooling is the most deleterious. Therefore, this paper places strong emphasis on minimizing the degrading effect of transverse velocities. In doing so we develop a general optimization scheme for achieving narrow lines that is suitable for pattern formation studies. The use of Rydberg atoms with large polarizabilities allows us to operate in the long wavelength regime, thus opening up the possibility of producing a single deposited line using a focusing lens whose period is larger than the atomic beam. Significantly, as the results below show, our optimization scheme makes it possible to create a single deposited line even when the atomic beam is bigger than the period of the focusing lens.

The article is organized as follows. Section II presents a brief overview of the laser-atom interaction and Sec. III provides details about the computational implementation of the atomic trajectories simulation and optimization algorithm. Section IV presents the results and discussions and Sec. V summarizes the paper and comments on future work.

II. THEORY

A. Atom-field interaction

We consider an atomic system interacting with a polychromatic standing wave (SW). Within the dipole approximation the light-plus-matter Hamiltonian reads

$$\hat{H} = \hat{K}(\mathbf{r}_{\mathrm{c.m.}}) + \hat{H}_{\mathrm{el}}(\mathbf{r}_{\mathrm{el}}) - \boldsymbol{\mu}(\mathbf{r}) \cdot E(\mathbf{r}_{\mathrm{c.m.}}, t), \tag{1}$$

where $\mathbf{r}_{\mathrm{c.m.}}$ is the atomic center-of-mass coordinate with associated kinetic energy operator $\hat{K}(\mathbf{r}_{\mathrm{c.m.}})$. The quantity $\hat{H}_{\mathrm{el}}(\mathbf{r}_{\mathrm{el}})$ is the Hamiltonian for the internal electronic motion where $\mathbf{r}_{\mathrm{el}}$ denotes the electronic coordinate. The interaction between the atom and the field is represented by the term $-\boldsymbol{\mu}(\mathbf{r}) \cdot E(\mathbf{r}_{\mathrm{c.m.}}, t)$, where $\boldsymbol{\mu}(\mathbf{r})$, $\mathbf{r} \equiv \{\mathbf{r}_{\mathrm{el}}, \mathbf{r}_{\mathrm{c.m.}}\}$, is the electric-dipole operator and $E(\mathbf{r}_{\mathrm{c.m.}} t)$ the electric field at the atom's center-of-mass position.

We make use of the adiabatic approximation to separate out the center-of-mass motion from the much faster electronic motion and obtain a Schrödinger equation for the electronic wave function which is parametrically dependent on $\mathbf{r}_{\mathrm{c.m.}}$,

$$i\hbar \frac{\partial}{\partial t} \Psi_{\mathrm{el}}(\mathbf{r}_{\mathrm{el}}, t; \mathbf{r}_{\mathrm{c.m.}}) = [\hat{H}_{\mathrm{el}}(\mathbf{r}_{\mathrm{el}}; \mathbf{r}_{\mathrm{c.m.}}) - \boldsymbol{\mu}(\mathbf{r}_{\mathrm{el}}; \mathbf{r}_{\mathrm{c.m.}}) \cdot \mathbf{E}(\mathbf{r}_{\mathrm{c.m.}}, t)] \Psi_{\mathrm{el}}(\mathbf{r}_{\mathrm{el}}, t; \mathbf{r}_{\mathrm{c.m.}}). \tag{2}$$

Since weak fields are employed, first order time dependent perturbation theory can be used to determine the electronic wave function,

$$\Psi_{\mathrm{el}}(\mathbf{r}_{\mathrm{el}}, t; \mathbf{r}_{\mathrm{c.m.}}) = \phi_i(\mathbf{r}_{\mathrm{el}}) e^{-i\omega_1 t} + \sum_{j \neq i} c_j(t; \mathbf{r}_{\mathrm{c.m.}}) \phi_j(\mathbf{r}_{\mathrm{el}}) e^{-i\omega_j t}, \tag{3}$$

where $\phi_j(\mathbf{r}_{\mathrm{el}})$ and $\hbar\omega_j$ are, respectively, eigenstates and eigenvalues of the field-free Hamiltonian $\hat{H}_{\mathrm{el}}(\mathbf{r}_{\mathrm{el}})$; $\phi_i(\mathbf{r}_{\mathrm{el}})$ is the initial state of the atom.

The polychromatic standing wave has an electric field of the form

$$\mathbf{E}(x,z,t) = \sum_{l=1}^{N} \mathbf{E}_l(x,z,t), \tag{4}$$

where $\mathbf{E}_l(x,z,t)$ is the sum of two counter-propagating cw fields,

$$\mathbf{E}_l(x,z,t) = \hat{\boldsymbol{\eta}}_l \frac{E_l^{(0)}}{2} \cos(k_l x + \phi_l) g(z) [\exp(-i\omega_l^F t) + \mathrm{c.c.}], \tag{5}$$

and $\hat{\boldsymbol{\eta}}_l$ denotes the polarization direction of the lth field, $g(z)$ is the laser beam profile, and c.c. denotes the complex conjugate of the term preceding it. N is the number of electric fields; in the majority of this paper $N=1$ or 2 suffice. The spatial part of the lth standing wave field is $F_l(x) \equiv \cos(k_l x + \phi_l)$. Figure 1 shows the laboratory coordinates used herein. The electric fields are polarized along the z axis and propagate along the x axis. The atom's center of mass moves in the (x,z) plane. The polarizations are taken to be parallel to one another and perpendicular to x, and to be aligned, as depicted in Fig. 1, along the laboratory frame z axis which is taken to be perpendicular to the surface. The electric fields are considered uniform along the y axis, thus the SW acts like an array of cylindrical lenses that focuses the atomic beam into a grating structure on the substrate. Three different laser profiles $g(z)$ were considered, as shown in Fig. 2. Note that in

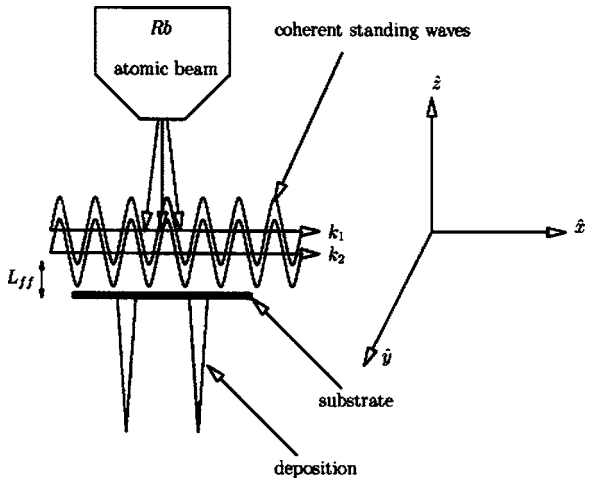

FIG. 1. A schematic representation of the lithographic experiment for Rb atomic beam in a Rydberg state interacting with a polychromatic standing wave.

subsequent equations, the coordinate of the center of mass $\mathbf{r}_{\text{c.m.}}$ will be replaced by (x,z).

In first order the coefficients c_j are given by

$$c_j(x,z,t) = -\sum_l \frac{E_l^{(0)}}{\hbar} F_l(x) g(z) \mu_{ji}^{(l)} \times \left[\frac{e^{i(\omega_{ji}+\omega_l^F - \Gamma_j/2)t}}{\omega_{ji}+\omega_l^F - i\Gamma_j/2} + \frac{e^{i(\omega_{ji}-\omega_l^F - \Gamma_j/2)t}}{\omega_{ji}-\omega_l^F - i\Gamma_j/2} \right], \quad (6)$$

where $\mu_{ji}^{(l)} = \langle \phi_j | \hat{\boldsymbol{\eta}}_l \cdot \boldsymbol{\mu} | \phi_i \rangle$ are the transition dipole moments and Γ_j the linewidths which account for the finite lifetime of excited states.

Substituting Eq. (6) into Eq. (3) and calculating the expectation value of the interaction term in Eq. (2), $\langle \Psi_{\text{el}}(\mathbf{r}_{\text{el}},t;x,z) | \boldsymbol{\mu} \cdot \mathbf{E}(x,z,t) | \Psi_{\text{el}}(\mathbf{r}_{\text{el}},t;x,z) \rangle$, we obtain, within the rotating wave approximation, an expression for the LIP,

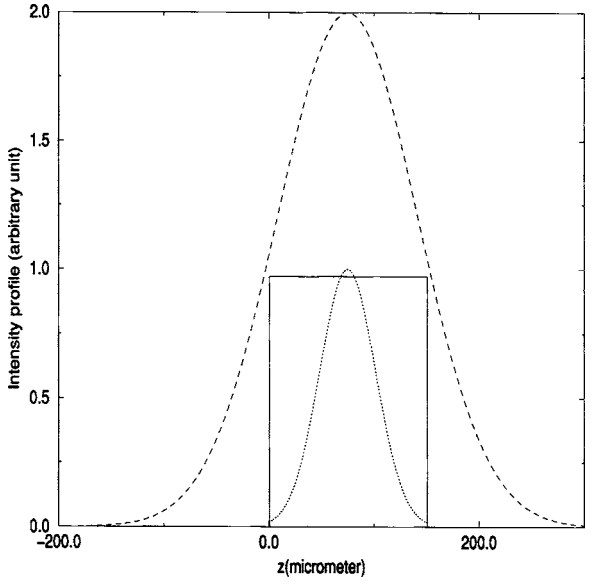

FIG. 2. Laser beam profiles: uniform (full line), Gaussian I (dotted line), and Gaussian II (dashed line).

$$V_{\text{LIP}}(x,z,t) = -\sum_l \frac{E_l^{(0)2}}{\hbar} F_l(x)^2 g(z)^2 \sum_j \mu_{ij}^{(l)} \mu_{ji}^{(l)} e^{-(\Gamma_i+\Gamma_j)t/2} \times \left[\frac{1}{\omega_{ji}-\omega_l^F - i\Gamma_j/2} + \frac{1}{\omega_{ji}+\omega_l^F - i\Gamma_j/2} \right] + \text{c.c.} \quad (7)$$

Altering the light-induced potential V_{LIP} allows one to manipulate the atomic trajectories, and hence the deposition pattern. V_{LIP} can be manipulated through coherent control by exploiting the interference between different optical excitation pathways.[17,19] It can also be altered by changing the parameters of the external electric fields, i.e., $E_l^{(0)}$ and $F_l(x)$ in Eq. (7).

Note that in order to arrive at Eq. (7), we utilize the particle's point of view to describe the light-plus-matter system semiclassically. Alternatively, one can use the dressed-atom picture[18] to treat the light-matter interaction. In this case, V_{LIP} can be interpreted as a position-dependent light (ac-Stark) shift due to a spatially varying light intensity, $F_l(x)$.[35] When a laser is well detuned from resonance, the atoms remain in the initial state, $\phi_i(\mathbf{r}_{\text{el}})$, and the light shift of this state plays the role of a potential energy, giving rise to a force which is equal and opposite to its gradient. An advantage of using the particles picture is that the theoretical formulation developed here can readily be generalized to molecules[17] and other laser-matter problems such as focusing and alignment of molecules.[12–14,34]

B. Polarizability of a Rydberg atom

Since the light-induced potential expressed in Eq. (7) is a product of the atom's induced dipole moment with the external field, i.e., $V_{\text{LIP}} = -\langle \boldsymbol{\mu}_{\text{ind}} \rangle \cdot \mathbf{E}(\mathbf{r}_{\text{c.m.}},t)$, the induced dipole moment is obtained by dividing V_{LIP} by the electric field of the laser light. Further factoring out the electric field from the induced dipole moment gives an expression for the dynamic (frequency dependent) polarizability,

$$\chi_i(\omega_l^F) = \frac{e^2}{\hbar} \sum_j \mu_{ij}^{(l)} \mu_{ji}^{(l)} \left[\frac{1}{\omega_{ji}+\omega_l^F - i\Gamma_j/2} + \frac{1}{\omega_{ji}-\omega_l^F - i\Gamma_j/2} \right]. \quad (8)$$

The transition dipole moments in this expression, $\mu_{ji}^{(l)}$, are calculated analytically by using the quantum defect theory developed by Kostelecky and Nieto.[28] We specialize the treatment by using hydrogeniclike wave functions $\langle \mathbf{r}_{\text{el}} | n,l,m \rangle$, where n, l, and m denote the effective principal, angular momentum, and magnetic quantum numbers, respectively. Reference 19 provides details for the computation of the dynamic polarizability of a Rydberg atom. The final expression is

$$\chi_{nlm}(\omega_l^F) = \frac{e^2}{\hbar} \sum_{n_e l_e m_e} |\langle n_e l_e | r | nl \rangle|^2 \frac{4\pi}{3} \frac{3(2l+1)(2l_e+1)}{4\pi} \Bigg) \times (-1)^{2m_e} \begin{pmatrix} 1 & l & l_e \\ 0 & m & -m_e \end{pmatrix}^2 \begin{pmatrix} 1 & l & l_e \\ 0 & 0 & 0 \end{pmatrix}^2 \times \left[\frac{1}{\omega_{ji} + \omega_l^F - i\Gamma_e/2} + \frac{1}{\omega_{ji} - \omega_l^F - i\Gamma_e/2} \right]. \quad (9)$$

Results calculated using this method were in good agreement with experimental results.[19] Note that the polarizability of rubidium Rydberg atoms is far larger than that of the ground state. As the results will show, this large polarizability allows one to obtain sharp deposited lines using relatively weak fields.

III. COMPUTATIONAL METHODOLOGY

A. Atomic density distribution

We use a semiclassical approximation to treat the light-plus-matter system. This approximation is valid because the extension of the atomic wave packet is small compared with the long wavelengths of the light employed in this work. Also, large detunings minimize the probability that an atom spontaneously emits a photon during its passage through the SW. Even if it happens, one or two photon recoils would have a negligible effect on the trajectory of an atom traveling at thermal speeds over a distance of laser beam radius. We note that the validity of the classical trajectory tracing method in nanolithography has already been demonstrated both theoretically and experimentally.[36]

Within the semiclassical treatment, the center of mass of each atom in a beam satisfies the classical equation of motion,

$$M \frac{\partial}{\partial t} x_i = p_i^x, \quad (10)$$

$$\frac{\partial}{\partial t} p_i^x = -\frac{\partial}{\partial x} V_{\mathrm{LIP}}(x,z,t) \Big|_{x_i}, \quad (11)$$

and

$$M \frac{\partial}{\partial t} z_i = p_i^z, \quad (12)$$

$$\frac{\partial}{\partial t} p_i^z = -\frac{\partial}{\partial z} V_{\mathrm{LIP}}(x,z,t) \Big|_{z_i}, \quad (13)$$

where the subscript i denotes the ith atom with the coordinates $(x_i(t), y_i(t), z_i(t))$, momenta (p_i^x, p_i^y, p_i^z), and mass M. Note that the light force along the y direction is assumed to be negligible as compared to those along the x and z directions. We consider two laser profiles: uniform, representing a sudden turn-on and turn-off of the laser, and Gaussian, representing an adiabatic turn-on and turn-off.

The above equations are solved for an ensemble of atomic trajectories to obtain the atomic density distribution $\rho(x,t)$. From a uniform initial spatial distribution of atoms, results are determined at time $t = t_{\mathrm{int}} + L_{\mathrm{ff}}/v_z$, where t_{int} is the atom-field interaction time, L_{ff} is the free-fall distance, i.e., dynamics in the absence of the field, and v_z is the longitudinal velocity.

The computation of the deposition pattern involves the following steps:

(1) At $t=0$, a fixed number of atoms is uniformly distributed over the nozzle segment of size X. This nozzle segment is subdivided into N cells of size $\Delta x = X/N$, where Δx is chosen sufficiently small so that the force at x_i, which is the gradient of the LIP, remains constant over the cell. In case of a perfectly collimated atomic beam (no transverse velocity) one atom is assigned to each cell. Otherwise $N_v = 100$ atoms are assigned to each cell. This number is large enough to describe the Maxwellian velocity distribution of the transverse velocity. The initial longitudinal velocity distribution is considered uniform. In case of a Gaussian beam profile, the longitudinal velocity spreads during the interaction of the atoms with the fields.

(2) Given a time t_0, the LIP is calculated at every point $(x_i, z_i) = (-X/2 + (n-1)\Delta x, z_i)$ $(n = 1, 2, \ldots, N)$. Hamilton's equations are solved to obtain $v_i^q = p_i^q/M$ $(q = x, z)$ at time $t = t_0 + \Delta t$. The Δt time step is chosen small enough to maintain energy conservation. Since there are no forces in the y direction, the v_i^y velocity components are constant (zero in this paper). Supplementing these values with the v_i^q information obtained from Hamilton's equations gives the atomic positions (x_i, y_i, and z_i) for each atom in the ensemble at time $t = t_0 + \Delta t$. The procedure is repeated until the atom hits the surface.

(3) After all the trajectories have terminated, the density of the atoms on the surface is analyzed by considering a segment of size $2X$. Histograms of the data provide the deposited atomic density.

B. Optimization methodology

Our objective is to find an optimal set of electric field parameters that produce sharp deposition patterns with little background while avoiding loss of population due to excess defocusing during the deposition. This objective is quantified in the target function,

$$F(T) = N_p(T) + \alpha h(T), \quad (14)$$

where N_p represents the number of particles that reach a predefined target region T of the surface and $h(T)$ is the height (as a number of trajectories) of the peak formed in that region. T often is the central region of the plate. By maximizing $F(T)$ we maximize the number of atoms that reach the target region, thus minimizing the loss of atomic population during the laser focusing. We also maximize the height of the deposited peak formed in that region. The weighting parameter α balances the importance of the height of a peak versus the atomic population in the target function. The best value of α, which was $\alpha = 1$, was found by trial and error.

The target function $F(T)$ depends on the electric field parameters and the experimental configuration. Particular parameters such as the state of the Rydberg atom, the interaction time, and the free-flight distance are fixed whereas the fields' intensities, frequencies, and phases [$E_i^{(0)}$, ω_l^F, and ϕ_l in Eq. (5)] are optimized. The optimization procedure is constructed for an electric field composed of N independent electric field contributions (usually $N=2$). Hence the target function is a function of $3N$ variables. The optimization starts from a guess for the initial $3N$ parameters and iterates to convergence using a modified Powell algorithm[37] to maximize $F(T)$.

In many optimal control scenarios the target function is a simple observable, e.g., the dissociation or ionization rate in a chemical process. Here the target function is derived from a complex observable, a deposition pattern, which is the result of a dynamical evolution. Hence a large number of target functions can be conceived. The target function used in this paper is the best found after much trial and error. For example, note that the width of the deposited peak, defined as the full width at half maximum, is not included explicitly in the target function. When a very sharp peak and a small pedestal are obtained, it means that the optimization procedure has found a good "focal length" for the lens represented by V_{LIP}. With a good focal length, the feature width of the deposited peak is also minimized.

For a simple case of atoms passing through one uniform electric field, whose intensity is in the focusing regime (see the next section for a definition of this regime), by using an analogy between laser-focused nanolithography and traditional optics one can derive an analytic expression for the focal length.[38] However, most cases in this paper are complex, involving one or two fields of uniform or Gaussian profiles. Furthermore, the deposition process can happen in the channeling regime,[39,40] which has no analogy in optics. Therefore, use of a numerical optimization methodology is necessary in order to obtain high-contrast, sharp deposition patterns.

Note that we found, as in most nonlinear problems, that the results converged to local minima that depend sensitively on the initial parameter guess. This is especially true of the wavelengths of the fields. Hence it was necessary to choose the wavelengths of the initial guess using physical intuition.

Finally, we remark that the free-fall distance L_{ff} is set to zero in all of our computations. Experimentally, L_{ff} is usually small. Note that if L_{ff} is chosen nonzero one can optimize the target function for the new experimental configuration.

IV. RESULTS AND DISCUSSIONS

For comparison purposes consider first a perfectly collimated atomic beam; a more realistic beam with finite transverse velocities will be considered later below. Both uniform and Gaussian laser profiles are used and results are compared for deposition controlled by monochromatic and by polychromatic lasers. This sequential approach also provides insight into the nature of the fields required to achieve narrow sharp lines. Far-detuned off-resonant fields are used in order to minimize the stimulated emission;[41] the term Γ_i in Eq. (7) is therefore neglected. In all cases the initial longitudinal velocity is taken as 500 m/s and the interaction time $t_{\mathrm{inter}}=0.3$ μs, which is less than the lifetimes of Rydberg states studied in this paper.

A. Perfectly collimated atomic beam

To see how the optimization proceeds, consider an example of the deposition patterns obtained during the optimization of the $8s$ Rb atomic beam traversing a laser beam consisting of two standing wave fields with an atomic beam width of 10 μm, shown in Fig. 3. In this case the optimization converged after three iterations. Panel (a) shows the deposition pattern resulting from the initial guess parameters, which is seen to consist of a noisy background with no distinct peak. After the first iteration step, in which all the six parameters are optimized, the deposition pattern improves considerably [panel (b)], now consisting of three sharp peaks and a much smaller background. The final deposition and the associated LIP are shown in panels (c) and (d), respectively. Comparison of panel (a) with panel (c) confirms that the optimization has considerably reduced the noise and increased the sharpness of the deposited peaks. Here the peaks are separated by $\lambda_1/2$, in accord with observations made previously[5,7,8] and are of width 10 nm. Sharper peaks can be obtained with further optimization, as discussed later below. Note that even though the two electric fields appear to have approximately the same wavelength, the first field produces a deeper light-induced potential because in the far off-resonant regime a large difference in the detuning does not result in a large difference in the wavelength. The first field's detuning, below the $8p$, $\Delta_1=5.21\times10^9$ Hz, is approximately three times smaller than the second's, $\Delta_2=14.8\times10^9$ Hz. This difference results in a deeper LIP for the first field because the dynamic polarizability in the region examined is approximately inversely proportional to the $8s$ to $8p$ detuning.

Since our goal is to produce a single peak within the plate size, i.e., between -10 and 10 μm, the two outer peaks in Fig. 3 are extraneous. There are three possible approaches to removing these peaks: (1) use a mechanical slit to deflect the portion of the atomic beam that forms the unwanted peaks,[42] (2) increase the fields' wavelengths, or (3) split the laser into two components so that one serves to defocus the unwanted part and the other to focus the remainder of the beam. Since our interest is in using light to manipulate the atoms, and since the mechanical slit loses a lot of incident flux, we focus upon items (2) and (3).

The idea of increasing the wavelengths arises from the fact that the two outer peaks are a consequence of the relative size of the wavelength and the plate. For a fixed Rydberg atom state, increasing the wavelength of the electric field results in a decrease in the dynamic polarizability and a shallower LIP, making laser focusing less effective. On the other hand, if one choose a state of higher principal quantum numbers n, then the spacing [i.e., ω_{ji} in Eq. (7)] between two adjacent energy levels become smaller which, for a given wavelength, decreases the detuning and increases the dy-

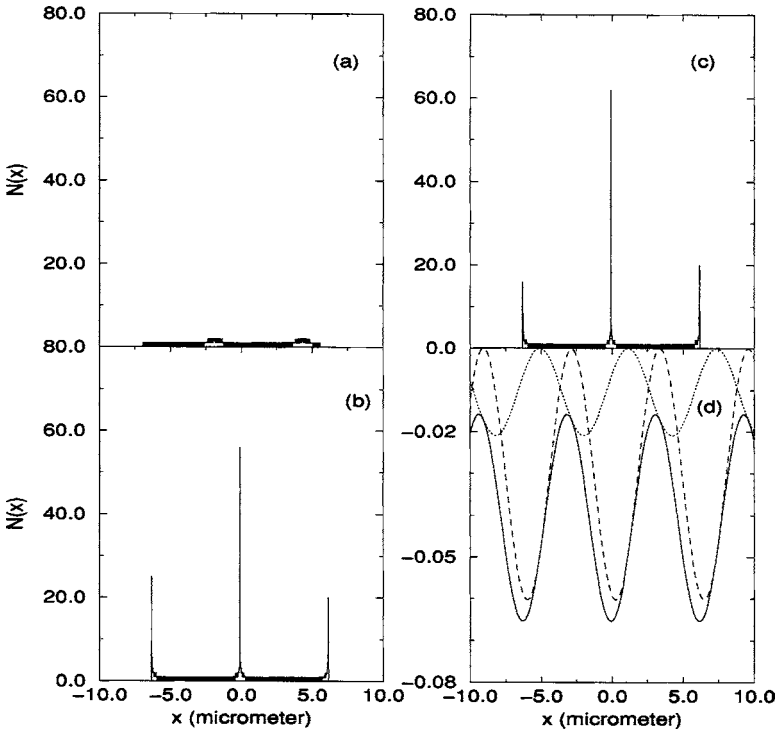

FIG. 3. The deposition patterns [(a)–(c)] in an optimization procedure and the light-induced potential (d) associated with the final deposition pattern. In (d) the dashed and dotted lines represent the LIP associated with the first and second fields, respectively. The full line represents the total LIP. The state of the Rydberg Rb atom is $8s$. The first field's parameters are $E_1=13$ W/cm^2, $\Delta_1=5.21\times10^9$ Hz, and $\lambda_1=12.4611$ μm. The second field's parameters are $E_2=13$ W/cm^2, $\Delta_2=14.8\times10^9$ Hz, and $\lambda_2=12.4618$ μm. The relative phase is $\Phi_F=\Phi_2-\Phi_1=1.13$ rad. 600 trajectories are simulated. The transverse velocity is taken as zero. The time of interaction $t_{\text{int}}=0.3$ μs.

namic polarizability. In short, Rydberg atoms of higher-lying excited states are useful in order to use longer wavelengths of light.

Note that Rydberg atoms have relatively long radiative lifetimes (τ) due to their small dipole coupling to the ground state and other low-lying states. For example, the $12s$ state studied extensively in this paper has a radiative lifetime of $\tau\approx0.75$ μs.[43] In order to minimize decay into the ground and other low-lying states, the interaction time is chosen so that $t_{\text{inter}}<\tau$. In this work $t_{\text{inter}}=0.3$ μs; it satisfies the just stated condition. Taking lifetimes and longer wavelengths of light into account, numerical experiments show that with $\lambda\approx70$ μm, which corresponds to far infrared regime, $n=10$ [$\tau\approx0.4$ μs (Ref. 43)] is the minimum in order to have an efficient laser focusing.

Figure 4 shows the results for the $12s$ state Rydberg Rb atomic beam passing through a standing wave field. The parameters are indicated in the figure caption. Panel (a) shows that there is now only one focusing center and that, consequently, the deposition pattern consists of only one peak [panel (b)]. In addition, the deposited peak is very sharp, being 1 nm wide, because of the harmonic characteristic of

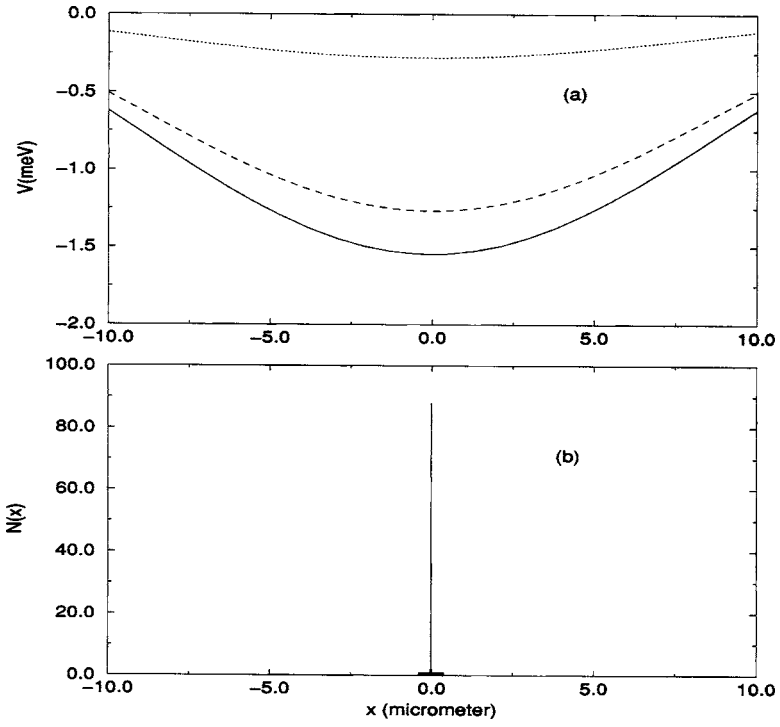

FIG. 4. The LIP (a) and the deposition pattern (b) of the $12s$ Rydberg Rb atomic beam. The beam size is 10 μm. The first field's parameters are $E_1=13.28$ W/cm^2, $\Delta_1=2.5\times10^9$ Hz, and $\lambda_1=70.8$ μm. The second field's parameters are $E_2=13.27$ W/cm^2, $\Delta_2=11.5\times10^9$ Hz and $\lambda_2=70.9$ μm. The relative phase is $\Phi_F=0$ rad. Explanation for panel (a) and other parameters are as in Fig. 3.

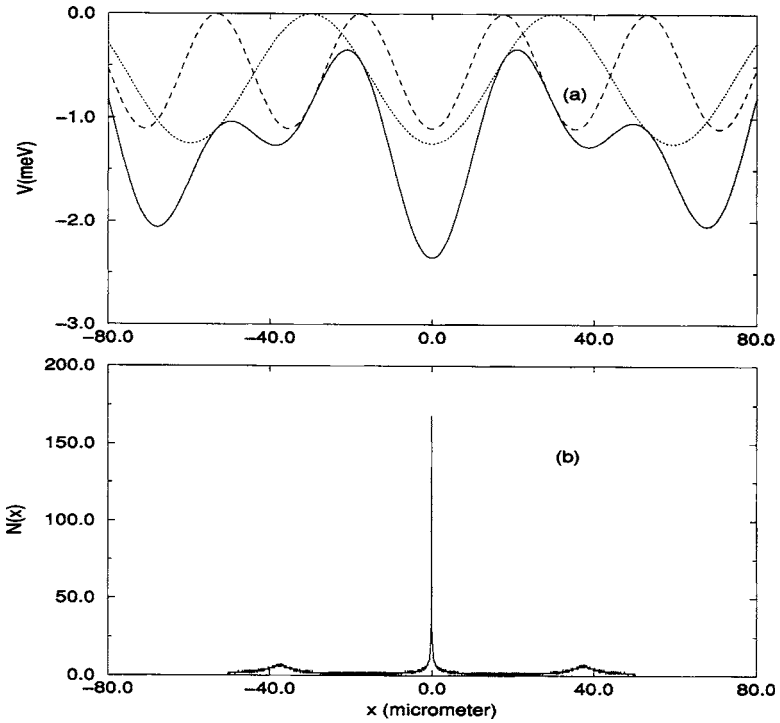

FIG. 5. The LIP (a) and deposition pattern (b) of the $12s$ Rydberg Rb atomic beam. The beam size is 100 μm. The first field's parameters are $E_1=13.27$ W/cm^2, $\Delta_1=2.92\times10^9$ Hz, and $\lambda_1=70.88$ μm. The second field's parameters are $E_2=8.88\times10^4$ W/cm^2, $\Delta_2=10.77\times10^{12}$ Hz, and $\lambda_2=119.1$ μm. The relative phase is $\Phi_F=0$ rad. 3000 trajectories are used. Explanation for panel (a) and other parameters are as in Fig. 3.

the LIP resulting from an iterative optimization scheme. That is, Fig. 4 results from a three-step optimization procedure. Initially we used a large target region in a central region of the plate, encompassing −2.5 to 2.5 μm. This target region resulted in a reasonably sharp peak and minimized the loss of flux. In the second and third steps, we further minimized the feature width by successively using smaller target regions ranging from −1 to 1μm and from −0.5 to 0.5μm, respectively. Calculations were performed using one and two fields with uniform intensity profile (Fig. 2, full line). All the converged results gave feature widths of 1 nm. Note that an attempt was made to use the smallest target region in one step for the calculations shown in Fig. 4, but the calculations did not converge. This three-step optimization procedure was developed in order to avoid such numerical difficulties.

In Figs. 3 and 4 the size of the atomic beam is 10 μm, which is smaller than the period of the LIP. Although experimental techniques are able to produce a beam as small as 5 μm by using a special miniature capillary micronozzle,[44] this method is associated with considerably reduced atomic flux. A wider atomic beam of 100 μm can be manufactured by using less stringent equipment and is more desirable. However, with such an atomic beam the optimized parameters obtained above would yield a deposition pattern consisting of several sharp peaks equally spaced on the substrate because the atomic beam is larger than the period of the LIP. Further increasing wavelength in order to restore the single sharp peak is not desirable because this requires a higher-lying Rydberg state or a more intense field. Both solutions increase the probability of field ionization, which degrades the deposition.

Rather than these approaches we consider a 100 μm wide beam interacting with a laser field comprising two components, i.e., focusing and defocusing lenses. The defocusing part causes some of the atomic trajectories to deflect off the plate, resulting in an acceptable loss of population. Figure 5 depicts the optimized LIP, in panel (a), and the resultant deposition pattern, in panel (b). The first field (dashed line), with optimized wavelength $\lambda_1=70.88$ μm, acts as a focusing lens, and the second field (dotted line), with optimized wavelength $\lambda_2=119.1$ μm, acts as a defocusing lens. A single, sharp deposited peak of 1 nm width is obtained. The contrast, defined as the ratio of the height of the deposited peak to the height of the pedestal, is 30:1, which is excellent. Note that here the size of the atomic beam is more than twice larger than the period of the focusing LIP.

To simulate a more realistic nanolithographic process a laser with a Gaussian profile[38,45] $g(z)=\exp(-2z^2/\sigma_z^2)$, where σ_z is the $1/e^2$ radius of the Gaussian laser beam, was also considered. Two Gaussian profiles were used: Gaussian I with $\sigma_z=70$ μm, which fits inside the formerly used uniform profile and Gaussian II with $\sigma_z=150$ μm, whose width matches the uniform profile. Both are illustrated in Fig. 2, along with the uniform profile. With a Gaussian profile, the atoms experience a force along the z direction that causes the atoms' longitudinal velocities to change along the z direction, resulting in a spread in the longitudinal velocity distribution. In addition, the LIP changes with respect to the uniform profile case. Reoptimization with these profiles, starting with the optimized uniform profile results, gives a sharp deposited peak that is, once again, 1 nm wide. Thus, optimized lines as narrow as 1 nm are possible in the absence of an initial transverse velocity distribution.

Note that red-detuned fields have been used throughout this paper. When a blue-detuned laser field is applied, its maxima serve as focusing centers and minima as defocusing centers. Calculations performed for blue-detuned fields yielded qualitatively similar deposition patterns to those above.

TABLE I. Feature widths (in nanometers) of the deposited peaks calculated with one field. The numbers in parentheses are the fields' wavelengths (in micrometers), phases (in radians), and intensities (in W/cm^2). The transverse temperature is 1 mK.

	Profile		
	Uniform	Gaussian I	Gaussian II
Low intensity	140	140	
	(70.874, 0, 13.34)	(70.871, 0, 12.89)	
High intensity	15	65	15
	(77.553, 0, 13.26×10^4)	(72.428, 0, 13.27×10^4)	(71.512, 0, 13.18×10^4)

B. Atomic beam with transverse velocities

Consider now the more realistic case where the atomic beam emerges with finite transverse velocities. Chromatic aberration due to the transverse velocities is the most deleterious, hence the optimization scheme is used to minimize their degrading effect. Chromatic aberration resulting from the longitudinal velocity spread, on the other hand, has a less degrading effect on the linewidth. Indeed, a longitudinal velocity spread as large as $\delta v_z/v_z \approx 1$ is expected to only broaden the line by 36% with respect to that obtained with a monochromatic beam.[38] Although not done here, we expect that the optimization scheme would minimize degrading effects due to the longitudinal velocity distribution of the incident atoms, as it has for the more deleterious longitudinal velocity spread arising from the Gaussian laser profile.

1. Optimized one field results

We consider the case where the beam is characterized by a thermal transverse velocity distribution of 1 mK, with the width of the velocity distribution $\delta=0.44$ m/s and maximum transverse velocity cutoff of 1.1 m/s. To enhance numerical efficiency, the optimization procedure begins with a perfectly collimated beam and uses the previously described multistep optimization procedure. After obtaining a sharp peak, whose width is usually 1 nm, transverse velocities are added and the system is optimized once again. Often this later optimization did not change the fields significantly. We first examine depositions in two laser intensity regimes: weak and moderately high intensities using one optimized laser. These results are summarized in Table I.

Figure 6 shows a few of the trajectories [panel (a)] and deposition pattern [panel (b)] in the weak intensity regime. The line broadening due to the atoms' initial transverse velocities can be estimated[17] as $\sqrt{2}t_{\mathrm{int}}\delta$, where t_{int} is the interaction time and δ is the width of the transverse velocity distribution. With $t_{\mathrm{int}}=0.3$ μs and $\delta=0.44$ m/s a width of 187 nm is obtained. Application of an optimized electric field yields only a somewhat narrower peak that is 140 nm wide.

Note that here the atomic trajectories show no oscillations in their path through the laser beam profile. Rather, the trajectories are simply focused onto a small portion of the plate. The results are said to lie in the focusing regime. On the other hand, if the LIP is such that the atoms oscillate

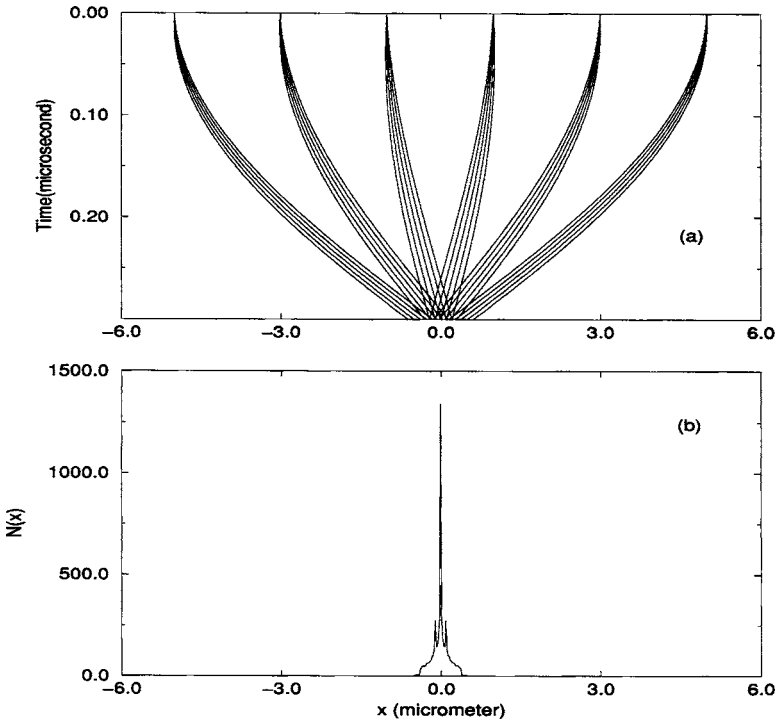

FIG. 6. Atomic trajectories (a) and the deposition pattern (b) of the 12*s* Rydberg Rb atom beam. The field's parameters are $E_1=13.34$ W/cm^2, $\lambda_1=70.875$ μm and $\Phi_F=0$ rad. 60 000 trajectories are simulated. The width of the transverse velocity distribution is $\delta=0.44$ m/s. The time of interaction $t_{\mathrm{int}}=0.3$ μs.

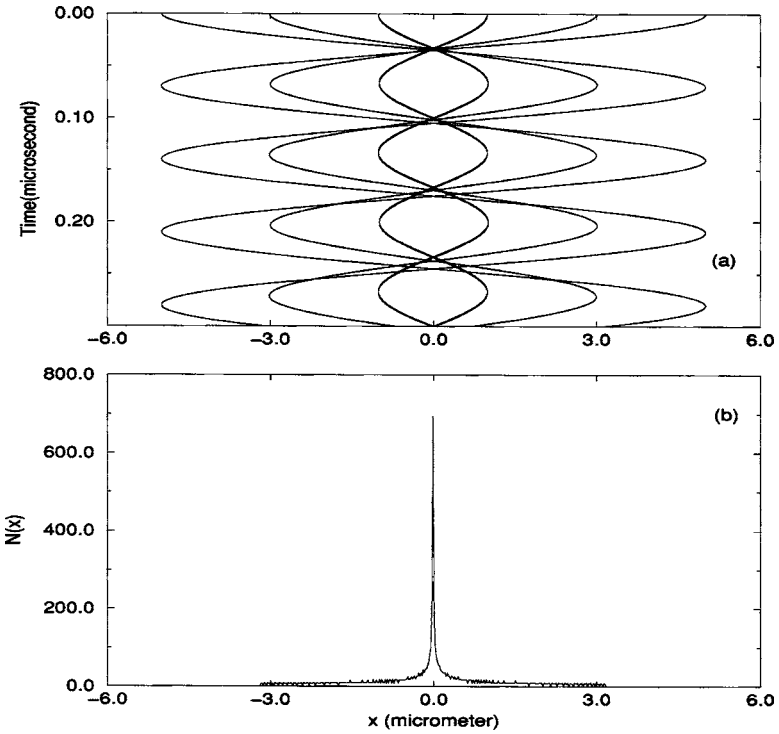

FIG. 7. Same as in Fig. 6 except that the field's parameters are $E_1=13.27\times10^4$ W/cm^2, $\lambda_1=71.533$ μm and $\Phi_F=0$ rad.

several times while traversing the laser beam, then the system is said to be in the so-called channeling regime. Channeling has in the past been used for laser cooling.[39,40] We see below that it is also a useful regime in which to operate in order to minimize the feature widths.

With an increase in the field's intensity, the LIP becomes steeper, resulting in a stronger dipole force and the atoms enter the channeling regime and oscillate within the potential well. Figure 7 illustrates the atomic trajectories and the associated deposition pattern. The channeling effect reduces the spreading of the transverse velocities, and a better focusing in both the position and transverse momentum spaces results; a feature of 15 nm width is now obtained. Narrower lines can be obtained upon further optimization, as discussed below.

Results are also shown in Table I using one field with a Gaussian profile. In the low field regime the field profile has no effect. In the higher intensity regime, Gaussian I shows a significantly larger width of 65 nm.

2. Optimized polychromatic results

Table II summarizes the optimized results obtained with a standing wave consisting of two fields, with the transverse velocity distribution as described above; these results are to be compared to those in Table I. The feature widths are given, along with the optimized field parameters. In the low intensity, or focusing regime, the one and two field results are quite similar, with the optimized feature width reduced slightly (from 140 to 130 nm) with the addition of the second field. However, in the high intensity, or channeling, regime, application of two fields reduces the line widths by a factor of 2. Hence, in the presence of a uniform or Gaussian II field, linewidths as small as 8 nm are obtained. For the narrower Gaussian field the line width can be reduced to 30 nm.

Two unsuccessful attempts at improvements are worth noting, as well as the effect of adding additional fields. First, small linewidths do not result in the case of Gaussian I profiles because the field region is very narrow. However, we cannot decrease the linewidth by increasing the field strength since the required fields would ionize the Rydberg atoms. Second, further increasing the Gaussian II beam's waist, to 250 μm, did not result in narrower lines. However, using three fields with uniform profile in the high intensity regime did reduce the feature width somewhat, from 8 to 6.5 nm. Hence, near-optimized narrow lines can be achieved with as few as two fields.

C. Experimental considerations

Rb atoms in Rydberg states can be prepared by optical excitation from the (5^2S) ground state.[27] To prepare the beam, Rb atoms are mixed with an inert buffer gas and the mixture is supersonically expanded through a nozzle to narrow down the translational velocity distribution. After exiting the nozzle, the supersonic Rb atom beam can be collimated by letting it pass through a series of slits[46] and/or by cooling the transverse velocity with a transverse laser field.[47] The Rydberg states are then prepared by laser excitation of the beam. To further ensure that well-defined Rydberg states are populated, the optical pumping and radiative deflection techniques developed in Ref. 48, wherein atoms are optically pumped and deflected before passing through collimating slits, can be used. By exploiting the high polarizability of the Rydberg atoms one can separate them from the ground-state atoms, thus reducing the background noise.

TABLE II. Same as in Table I except that two fields are used.

	Profile		
	Uniform	Gaussian I	Gaussian II
Low intensity	130	120	
	(70.876, 0, 13.28)	(70.872, 0, 13.28)	
	(70.9, 0, 13.27)	(70.9, 0, 13.27)	
High intensity	8	30	8
	(71.077, 0, 8.76×10^4)	(70.93, 0, 8.76×10^4)	(71.046, 0, 8.82×10^4)
	(71.162, 0, 13.26×10^4)	(71.162, 0, 12.99×10^4)	(71.162, 0, 13.27×10^4)

Rydberg atoms are chosen here for their large polarizabilities, making it is easier to produce a deep LIP with a relatively weak field (here less than 10^5 W/cm^2). This reduction in the intensity allows the use of cw lasers to focus the atomic beam, thus increasing the write rate by many orders of magnitude when compared to a pulsed laser.[14] Furthermore, with a cw laser we also minimize the problem of background atoms depositing on the substrate when the laser is off. By contrast, use of non-Rydberg atoms would require a far more intense field to produce a sufficiently deep potential well. For example, a perfectly collimated beam of atoms in the ground state requires a field intensity of 10^{13} W/cm^2.[49]

The large Rydberg atom polarizability results from the fact that electrons in high-lying Rydberg states are loosely bound to the ion core and hence they can be easily polarized by a laser field. At the same time, a strong field can certainly ionize the loosely bound Rydberg electrons. Therefore, care must be taken not to ionize the Rydberg atoms during the laser focusing, especially in the channeling regime where the field intensity is moderately intense. However, using the quasistatic model of Ref. 27 we can estimate the upper limit allowed for the field intensity. Using $n^*=8.865$ gives $E_{\text{ion}}=5\times10^6$ V/m as the allowed maximum, well above the most intense field that are used here [$\approx1\times10^6$ V/m].

The Rydberg atom's unusual large size would decrease the resolution of the deposition pattern. Specifically, a 12s state atom is $\approx$7.6 nm in diameter, comparable to the width of the deposited lines. However, the size of the Rydberg atom is greatly reduced by tunneling ionization once it approaches to within $\approx3.7n^2a_0$ of the surface.[50,51] The deposited ion would then be neutralized by interactions with the surface. The distance at which the ionization occurs is ≈0.3 μm, which is far shorter than the interaction distance of >100 μm in our model. Hence the tunneling ionization would not affect the LIP.

Throughout this work it is assumed that all atoms that hit the surface stick and do not migrate. Experimentally observed linewidths are, however, typically a factor of 2 larger than the calculated linewidths.[36] This discrepancy can likely be attributed to the neutralization of the ionized atoms, diffusion, aggregation, and growth of the atoms deposited on the surface. While a qualitatively clear picture of the line-broadening mechanism is yet to be developed, it is generally agreed that surface growth and diffusion play the most important role in nanostructure formation on the surface.[36,52,53]

Ideally, the surface diffusion coefficient of the deposited atoms must be small enough to maintain the fidelity of the deposition pattern. In practice, it can be reduced by increasing the deposition rate.[52] However, the high atomic flux associated with a large deposition rate can degrade the LIP because of the absorption in SW. Large detunings employed in this work minimize the deleterious effect of absorption, thus making use of a high deposition rate possible.

The diffusion coefficient also depends on the amount of the atoms deposited on the surface.[36] At the beginning of the deposition process, high mobility of Rb atom on the substrate can cause a large broadening of the linewidths. As more atoms accumulate, the diffusion coefficient decreases because of a lower mobility of Rb atoms on the Rb surface. Consequently the line-broadening effect is minimized. Once a significant amount of atoms is deposited on the surface, the linewidths will, however, increase again due to an increase in rubidium grain size with the thickness of the position pattern.

In future work, the deposition rate, the amount of the deposited atoms, and other important diffusion-and growth-related parameters such as the surface temperature and the atoms' longitudinal kinetic energies can be incorporated into our optimization algorithm in order to provide a robust technique for nanofabrication.

V. SUMMARY

These results show that it is possible to utilize relatively weak multifrequency long wavelength light, incident on Rydberg atoms, to produce a single narrow deposition line over a wide target region. By using a focusing and a defocusing field as part of a two-component electric field the single line can be successfully retained, even if the atomic beam is considerably larger than the width of the laser-induced deposition. Furthermore, polychromatic fields have been shown to allow for an optimization that successfully reduces the linewidth due to the transverse beam velocity distribution.

ACKNOWLEDGMENTS

We thank Photonics Research Ontario and the Natural Sciences and Engineering Research Council of Canada for support of this research.

[1] For a review see T. Ito and S. Okazaki, Nature (London) **406**, 1027 (2000).
[2] A. S. Bell, T. Pfau, U. Drodofsky, J. Stuhler, T. Schulze, B. Brezger, S. Nowak, and J. Mlynek, Microelectron. Eng. **42**, 587 (1998).
[3] F. Lison, H. J. Adams, D. Haubrich, M. Kreis, S. Nowak, and D. Me-

schede, Appl. Phys. B: Lasers Opt. **65**, 419 (1997).
[4] K. K. Berggren, R. Younkin, E. Cheung, M. Prentiss, A. J. Black, G. M. Whitesides, D. C. Ralph, C. T. Black, and M. Tinkham, Adv. Mater. (Weinheim, Ger.) **9**, 52 (1997).
[5] J. H. Thywissen, K. S. Johnson, R. Younkin, N. H. Dekker, K. K. Berggren, A. P. Chu, M. Prentiss, and S. A. Lee, J. Vac. Sci. Technol. B **15**, 2093 (1997).
[6] A. S. Bell, B. Brezger, U. Drodofsky, S. Nowak, T. Pfau, J. Stuhler, T. Schulze, and J. Mlynek, Surf. Sci. **435**, 40 (1999).
[7] C. C. Bradley, W. R. Anderson, J. J. McClelland, and R. J. Celotta, Appl. Surf. Sci. **141**, 210 (1999).
[8] J. J. McClelland and R. J. Celotta, Thin Solid Films **367**, 25 (2000).
[9] G. Timp, R. E. Behringer, D. M. Tennant, J. E. Cunningham, M. Prentiss, and K. K. Berggren, Phys. Rev. Lett. **69**, 1636 (1992).
[10] U. Drodofsky, M. Drewsen, T. Pfau, S. Nowak, and J. Mlynek, Microelectron. Eng. **30**, 383 (1996).
[11] V. I. Balykin and V. S. Letokhov, *Atom Optics with Laser Light* (Harwood Academic, Chur, Switzerland, 1995).
[12] T. Seideman, J. Chem. Phys. **106**, 2881 (1997).
[13] T. Seideman, Phys. Rev. A **56**, R17 (1997).
[14] R. J. Gordon, L. Zhu, W. A. Schroeder, and T. Seideman, J. Appl. Phys. **94**, 669 (2003).
[15] B. Dubetsky and P. R. Berman, Phys. Rev. A **58**, 2413 (1998).
[16] L. E. Helseth, Opt. Commun. **212**, 343 (2002).
[17] B. Dey, M. Shapiro, and P. Brumer, Phys. Rev. Lett. **85**, 3125 (2000).
[18] M. Shapiro and P. Brumer, *Principles of the Quantum Control of Molecular Processes* (Wiley, New Jersey, 2003).
[19] N. A. Nguyen, B. Dey, M. Shapiro, and P. Brumer, J. Phys. Chem. A **108**, 7878 (2004).
[20] T. P. Softley, Int. Rev. Phys. Chem. **23**, 1 (2004).
[21] G. Raithel, M. Fauth, and H. Walther, Phys. Rev. A **47**, 419 (1993).
[22] G. Raithel and M. Fauth, J. Phys. B **28**, 1687 (1995).
[23] Y. Yamakita, S. R. Procter, A. L. Goodgame, T. P. Softley, and F. Merkt, J. Chem. Phys. **121**, 1419 (2004).
[24] A. L. Goodgame and T. P. Softley, J. Phys. B **32**, 4839 (1999).
[25] D. Townsend, A. L. Goodgame, S. R. Procter, S. R. Mackenzie, and T. P. Softley, J. Phys. B **34**, 439 (2001).
[26] O. Kritsun, O. Boiko, and H. Metcalf, Bull. Am. Phys. Soc. **49**, 28 (2004).
[27] T. F. Gallagher, *Rydberg Atoms* (Cambridge University Press, Cambridge, 1994).
[28] V. A. Kostelecky and M. M. Nieto, Phys. Rev. A **32**, 3243 (1985).
[29] A. E. Bryson and Y. Ho, *Applied Optimal Control* (Hemisphere, Washington, D.C., 1975).
[30] A. P. Peirce, M. A. Dahleh, and H. Rabitz, Phys. Rev. A **37**, 4950 (1988).
[31] A. Assion, T. Baumert, M. Bergt, T. Brixner, B. Kiefer, V. Seyfried, M. Strehle, and G. Gerber, Science **282**, 919 (1998).
[32] R. J. Levis, G. M. Menkir, and H. Rabitz, Science **292**, 709 (2001).
[33] T. C. Weinacht, J. Ahn, and P. H. Bucksbaum, Nature (London) **397**, 233 (1999).
[34] A. Ben Haj-Yedder, A. Auger, C. M. Dion, E. Cances, A. Keller, C. Le Bris, and O. Atabek, Phys. Rev. A **66**, 063401 (2002).
[35] C. Cohen-Tannoudji, in *Fundamental Systems in Quantum Optics*, Les Houches Seisson LIII, edited by J. Dalibard, J. M. Raimond, and J. Zinn-Justin (Elsevier, Amsterdam, 1992).
[36] W. R. Anderson, C. C. Bradley, J. J. McClelland, and R. J. Celotta, Phys. Rev. A **59**, 2476 (1999).
[37] W. H. Press, B. P. Flannery, S. A. Teukolsky, and W. T. Vetterling, *Numerical Recipes in Fortran* (Cambridge University Press, Cambridge, 1992).
[38] J. J. McClelland, J. Opt. Soc. Am. B **12**, 1761 (1995).
[39] C. Salomon, J. Dalibard, A. Aspect, H. Metcalf, and C. Cohen-Tannoudji, Phys. Rev. Lett. **59**, 1659 (1987).
[40] V. I. Balykin, V. S. Letokhov, Y. B. Ovchinnikov, and S. V. Shulga, Opt. Commun. **77**, 152 (1990).
[41] Controllable stimulated emission can be exploited to enhance the deposition. See, e.g., K. S. Johnson, J. H. Thywissen, N. H. Dekker, K. K. Berggren, A. P. Chu, R. Younkin, and M. Prentiss, Science **280**, 1583 (1998).
[42] K. Totsuka, H. Ito, K. Suzuki, K. Yamamoto, M. Ohtsu, and T. Yatsui, Appl. Phys. Lett. **82**, 1616 (2003).
[43] C. E. Theodosiou, Phys. Rev. A **30**, 2881 (1984).
[44] J. Braun, P. K. Day, J. P. Toennies, G. Witte, and E. Neher, Rev. Sci. Instrum. **68**, 3001 (1997).
[45] M. Mutzel, D. Haubrich, and D. Meschede, Appl. Phys. B: Lasers Opt. **70**, 689 (2000).
[46] N. Ramsey, *Molecular Beams* (Clarendon, Oxford, 1956).
[47] B. Sheehy, S.-Q. Shang, P. van der Strater, and H. Metcalf, Chem. Phys. **145**, 317 (1990).
[48] P. L. Gould, G. A. Ruff, P. J. Martin, and D. E. Pritchard, Phys. Rev. A **36**, 1478 (1987).
[49] N. A. Nguyen, M. Shapiro, and P. Brumer (unpublished).
[50] J. Burgdörfer, P. Lerner, and F. W. Meyer, Phys. Rev. A **44**, 5674 (1991).
[51] S. B. Hill, C. B. Haich, Z. Zhou, P. Nordlander, and F. B. Dunning, Phys. Rev. Lett. **85**, 5444 (2000).
[52] R. E. Behringer, V. Natarajan, and G. Timp, Appl. Surf. Sci. **104/105**, 291 (1996).
[53] E. Jurdik, Th. Rasing, H. van Kempen, C. C. Bradley, and J. J. McClelland, Phys. Rev. B **60**, 1543 (1999).